



Mathematical Modeling of Reactive Fluid Flow in Solid Rocket Motor Combustion Chamber with/without Nozzle

{A. M. Hegab^{*}, S. A. Wilson, W. A. Elaskary, S. M. El-Behery, K. A. Yousif}[†]

Abstract: In the present work, a complete simulation of reactive flow in the combustion chamber of a rocket motor equipped with convergent-divergent nozzle has been introduced. The model describes the combustion process inside the combustion chamber considering a steady premixed reactant gas injected through side porous walls of the combustion chamber. The products flow through a convergent-divergent nozzle with adiabatic impermeable walls. The reactants are treated as two-dimensional, multi-components, turbulent compressible flow. The local properties of the mixture are calculated and updated during the solution process. At the boundary of the combustion chamber, a constant mass flux and predefined properties are considered. The proposed model employs the basic conservation equations of continuity, momentum and energy as well as the finite rate of reaction and species transport equations. Finite volume method is used to solve the basic nonlinear partial differential equations numerically. The details of the numerical scheme, structure of the used grids, numerical accuracy and stability are introduced. The effect of grid resolution as well as the validity of the results is included. The results showed fair agreement with other models in the literature; specially the reaction zone depth, temperature contours and species concentration along the entire space of the combustion chamber.

Keywords: Solid Propellant, Sandwich Propellant, Diffusion and Premixed Flames, Convergent and Divergent Nozzle, Reactive Flow in Rockets.

1. Introduction

Combustion process plays an important role in governing the gas flow inside the combustion chamber of solid rocket motor (SRM) which in turn controls the overall performance. The mixing process and reaction rate of the fuel and oxidizer exhibit clear effect on some important phenomena like combustion instabilities and acoustic waves generated and traveled along the combustion chamber. Many investigators [1-4] tried to emulate the solid fuel combustion by using paraffin hydrocarbons fuel as methane CH₄ and propane C₃H₈, while the air is used as oxidizer. Two different fuel/oxidizer configurations may be used in SRM. The first one depends on mixing of the fuel powder with the oxidizer grains at specified equivalence ratio. This method gives premixed flame which is characterized by fast reaction rate, high peak temperature and more uniform temperature gradient inside the combustion chamber. In second configuration, the fuel and oxidizer blocks arrange side by side in a manner that each fuel block is surrounded by two oxidizer blocks as a sandwich. The combustion occurs at the interface surface between the fuel and oxidizer.

^{*} Professor, corresponding author, Hegab2002us@yahoo.com .

[†] Mechanical Power Engineering Department, Faculty of Engineering, Menoufiya University, Shebin El-Kom, EGYPT.

This arrangement gives diffusion flame which is characterized by relatively slower reaction rate, deeper flame zone and non-regular surface topography of the solid reactants. Another important trial to simulate integral rocker ram-jet (IRR) is presented by Cherng et al. [5]. In their work, they introduced a mathematical model to simulate the turbulent diffusion combustion in IRR propulsion system. They indicated the importance of the design parameters on the propulsion efficiency. In the present work, a comprehensive code is developed to simulate the combustion process and gas flow inside the combustion chamber of the solid rocket. The code is capable to simulate the combustion process at different combustion modes (premixed, diffusion) and different flow regimes (laminar and turbulent). The model is validated by comparing its results with other published data [1, 2].

2. Mathematical Model

In the present work, a mathematical model for simulating the combustion process in SRM combustion chamber is introduced. The model is based on employing the strongly coupled set of nonlinear partial differential equations representing the conservation equations of mass and momentum in addition to a suitable turbulence model to compute the turbulence viscosity. The energy equation and the transport of species along the combustion chamber are also included. The model is used to address the effect of combustion mode on the flow pattern inside the combustion chamber, so both premixed and diffusion combustion are modeled. The flow inside the combustion chamber is treated as two-dimensional, compressible (laminar or turbulent) at steady state conditions. The mathematical representation of the model is summarized in the following subsections.

Continuity Equation

$$\frac{\partial \rho}{\partial t} + \frac{\partial \rho u_i}{\partial x_i} = 0.0 \quad (1)$$

Momentum Equation

$$\frac{\partial \rho u_i}{\partial t} + \frac{\partial \rho u_i u_j}{\partial x_j} = -\frac{\partial p}{\partial x_i} + \frac{\partial}{\partial x_j} \left(\mu_{eff} \left(\frac{\partial u_i}{\partial x_j} + \frac{\partial u_j}{\partial x_i} - \frac{2}{3} \delta_{ij} \frac{\partial u_k}{\partial x_k} \right) \right) \quad (2)$$

where, u_i and u_j are the streamwise (i-direction) velocity and the normal to main flow (j-direction) velocity, respectively. δ_{ij} is the Kronecker's delta function ($\delta_{ij}=1$ if $i=j$ and $\delta_{ij}=0$ if $i \neq j$). The effective viscosity is obtained from: $\mu_{eff} = \mu_l + \mu_t$; where μ_l is the laminar viscosity and μ_t is the turbulent viscosity, which needs a suitable turbulence model.

Turbulence Modeling

The modified version of $v^2 - f$ model of Lien and Kalitzen [6] and successfully used recently by El-Askary et al. [7] will be considered here. The distinguishing feature of the $v^2 - f$ model is its use of the velocity scale, v^2 instead of the turbulent kinetic energy, k , for evaluating the eddy viscosity. v^2 , which can be thought of as the velocity fluctuation normal to the streamlines, has shown to provide the right scaling in representing the damping of turbulent transport close to the wall, a feature that k does not provide.

The distribution of the turbulent viscosity is calculated from:

$$\mu_t = \rho C_\mu v^2 Time \quad (3)$$

where $Time$ is the turbulent time scale and given by:

$$Time = \max \left[\frac{k}{\varepsilon}, 6 \sqrt{\frac{\mu}{\rho \varepsilon}} \right] \quad (4)$$

The standard $k - \varepsilon$ equations are

$$\frac{\partial}{\partial x_j} (\rho u_j k) = \frac{\partial}{\partial x_j} \left[\left(\mu + \frac{\mu_t}{\sigma_k} \right) \frac{\partial k}{\partial x_j} \right] + \rho (P_r - \varepsilon) \quad (5)$$

$$\frac{\partial}{\partial x_j} (\rho u_j \varepsilon) = \frac{\partial}{\partial x_j} \left[\left(\mu + \frac{\mu_t}{\sigma_\varepsilon} \right) \frac{\partial \varepsilon}{\partial x_j} \right] + \frac{\rho}{Time} (C_{1\varepsilon} P_r - C_{2\varepsilon} \varepsilon) \quad (6)$$

where P_r and ε represent the production rate and the dissipation rate of the turbulent kinetic energy, k , respectively; while σ_k and σ_ε are model constants. The production rate is related to the mean strain of the velocity field through the Boussinesq assumption. That is,

$$P_r = \mu_t S^2 \quad (7)$$

where S is defined as:

$$S = \sqrt{\frac{1}{\rho} \left(\frac{\partial u_j}{\partial x_i} + \frac{\partial u_i}{\partial x_j} - \frac{2}{3} \delta_{ij} \frac{\partial u_k}{\partial x_k} \right) \frac{\partial u_i}{\partial x_j}} \quad (8)$$

The v^2 transport equation is

$$\frac{\partial}{\partial x_j} (\rho u_j v^2) = \frac{\partial}{\partial x_j} \left[\left(\mu + \frac{\mu_t}{\sigma_k} \right) \frac{\partial v^2}{\partial x_j} \right] + \rho (k f - 6 v^2 \frac{\varepsilon}{k}) \quad (9)$$

and the elliptic-relaxation equation f can be represented as:

$$L^2 \frac{\partial^2 f}{\partial x_j^2} - f = \frac{1}{T} \left[(C_1 - 6) \frac{v^2}{k} - \frac{2}{3} (C_1 - 1) \right] - C_2 \frac{P_r}{k} \quad (10)$$

and the turbulent length scale L is determined from the values of k and ε as follows:

$$L = C_L \max \left[\frac{k^{3/2}}{\varepsilon}, C_\eta \frac{(\mu/\rho)^{3/4}}{\varepsilon^{1/4}} \right] \quad (11)$$

The constants of the model are given as follows; see El-Askary et al. [7]:

$$C_\mu = 0.22; \sigma_k = 1; \sigma_\varepsilon = 1.3; C_{1\varepsilon} = 1.4(1 + 0.05\sqrt{k/v^2}); C_{2\varepsilon} = 1.9; C_1 = 1.4; C_2 = 0.3; \\ C_L = 0.23; C_\eta = 70. \quad (12)$$

As noticed, all model constants are completely wall-distance independent, see El-Askary et al. [7].

Energy Equation

$$\frac{\partial}{\partial t} \left(\rho \left(h + \frac{1}{2} V^2 - \frac{p}{\rho} \right) \right) + \frac{\partial}{\partial x_i} \left[\rho u_i \left(h + \frac{1}{2} V^2 \right) \right] = \frac{\partial}{\partial x_j} \left[k_{eff} \frac{\partial T}{\partial x_j} + u_i (\tau_{ij})_{eff} \right] + S_R \quad (13)$$

where, k_{eff} is the effective thermal conductivity and $(\tau_{ij})_{eff}$ is the effective stress tensor. The enthalpy of gas h is computed from:

$$h = \sum_{i=1}^N Y_i h_i \quad (14)$$

and the specific enthalpy of species i

$$h_i = \int_{T_{ref}}^T C_{pi} dT \quad (15)$$

The effective thermal conductivity is defined as:

$$k_{eff} = k + \frac{C_p \mu_t}{Pr_t} \quad (16)$$

where, C_p is the specific heat at constant pressure and Pr_t is the turbulent Prandtl number.

Species Equation

The species transport equations for different reactive components can be written as:

$$\frac{\partial \rho Y_i}{\partial t} + \frac{\partial \rho u Y_i}{\partial x} + \frac{\partial \rho v Y_i}{\partial y} = \frac{\partial}{\partial x} \left(D_{eff,i} \frac{\partial Y_i}{\partial x} \right) + \frac{\partial}{\partial y} \left(D_{eff,i} \frac{\partial Y_i}{\partial y} \right) + S_i \quad (17)$$

In the above equation Y_i is the local mass fraction of species i . In the present study N species are considered, namely the fuel, oxygen, carbon dioxide, water vapor and nitrogen respectively. To ensure species conservation, only four transport equations are solved, while the fifth species which is nitrogen is calculated as follows:

$$Y_{N_2} = 1 - (Y_f + Y_{O_2} + Y_{CO_2} + Y_{H_2O}) \quad (18)$$

where f denotes to the fuel, which in our case of study represents the methane CH_4 or propane C_3H_8 . The effective diffusion coefficient $D_{eff,i}$ can be calculated as follows:

$$D_{eff,i} = \rho D_{im} + \frac{\mu_t}{Sc_t} \quad (19)$$

The second term accounts the effect of turbulence on the diffusion of species. In laminar flow, this term is vanished.

Methane Combustion

In the current model validation, single-step kinetic reaction of methane combustion is considered as proposed in [1]. The stoichiometric combustion equation is as follows:



The source term of each species is calculated from the following finite rate equations [1].

$$S_{CH_4} = -1.3 \times 10^8 \exp\left(\frac{-E_a}{R_u T}\right) \rho Y_{CH_4}^{-0.3} Y_{O_2}^{1.3} \left(\frac{M_{CH_4}}{M_{O_2}}\right)^{1.3} \quad (21)$$

$$S_{O_2} = 2 \left(\frac{M_{CH_4}}{M_{O_2}}\right) S_{CH_4} \quad (22)$$

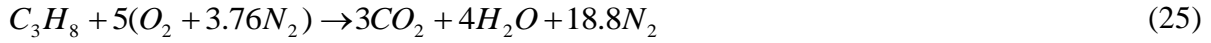
$$S_{CO_2} = -1 \left(\frac{M_{CH_4}}{M_{CO_2}}\right) S_{CH_4} \quad (23)$$

$$S_{H_2O} = -2 \left(\frac{M_{CH_4}}{M_{H_2O}}\right) S_{CH_4} \quad (24)$$

The activation energy E_a is 30 kcal/mole [1] and R_u is the universal gas constant.

Propane Combustion

The second validation case is based on premixed propane flame in 2D duct [2]. The stoichiometric single-step combustion is as follows:



The source term of each species is calculated from the following finite rate equations [2].

$$S_{C_3H_8} = -4.836 \times 10^9 \exp\left(\frac{-E_a}{R_u T}\right) \rho^{1.75} \left(\frac{Y_{C_3H_8}}{M_{C_3H_8}}\right)^{0.1} \left(\frac{Y_{O_2}}{M_{O_2}}\right)^{1.65} M_{C_3H_8} \quad (26)$$

$$S_{O_2} = 5 \left(\frac{M_{C_3H_8}}{M_{O_2}}\right) S_{C_3H_8} \quad (27)$$

$$S_{CO_2} = -3 \left(\frac{M_{C_3H_8}}{M_{CO_2}}\right) S_{C_3H_8} \quad (28)$$

$$S_{H_2O} = -4 \left(\frac{M_{C_3H_8}}{M_{H_2O}}\right) S_{C_3H_8} \quad (29)$$

The energy source term is calculated by

$$S_R = \sum_{i=1}^N S_i h_f^0 \quad (30)$$

where h_f^0 is the enthalpy of formation at reference temperature, Tref.

The specific heat of gas mixture is calculated as:

$$C_p = \sum_{i=1}^N Y_i C_{pi} \quad (31)$$

where

$$C_{pi} = \sum_{j=0}^4 a_{ji} T^j \quad (32)$$

The coefficients of specific heat polynomial for different species are given in Table (1).

Table (1) Polynomial coefficients of specific heat [8]

Species	Temperature range	a_0	a_1	a_2	a_3	a_4
O2	300-5000	811.1803	0.4108345	-0.0001750725	3.757596e-08	-2.973548e-12
N2	300-5000	938.8992	0.3017911	-8.109228e-05	8.263892e-09	-1.537235e-13
H2O	300-5000	1609.791	0.740494	-9.129835e-06	-3.813924e-08	4.80227e-12
CO2	300-1000	429.9289	1.874473	-0.001966485	1.297251e-06	-3.999956e-10
	1000-5000	841.3765	0.5932393	-0.0002415168	4.522728e-08	-3.15313e-12
C3H8	300-1000	169.1106	5.032259	0.001024072	-4.008482e-06	1.74279e-09
	1000-5000	1418.847	3.561693	-0.001184807	1.730731e-07	-9.073593e-12
CH4	300-1000	403.5847	9.057335	-0.01442509	1.580519e-05	-6.343051e-09
	1000-5000	872.4671	5.305473	-0.002008295	3.516646e-07	-2.33391e-11

The effect of fluid turbulence on the finite rate of reaction kinetics is considered as described in modified Eddy Breakup model 'EBU' [10], which was proposed originally by Spalding [11, 12]. In this model the effect of turbulence appears clearly on chemical reaction due to the local vortex stretching. So, the reaction rates in the case of turbulent combustion are calculated as the minimum of rates calculated from Arrhenius law (S_1) and that calculated by EBU model (S_2) as follows:

S_1 =Arrhenius law (Equations 21 and 26)

$$S_2 = C_R \rho \min \left| Y_f, \frac{Y_{O_2}}{r_1} \right| \frac{\varepsilon}{k} \quad (33)$$

$$S_f = -\min |S_1, S_2| \quad (34)$$

where, $C_R = 3$ [9] and $r_1 = 3.5(M_{O_2}/M_f)$

Equation of State

Finally, the equation of state determines the density distribution of the gas mixture from the pressure, temperature and species mass fraction:

$$P = \rho R_u T \sum_{i=1}^N Y_i / M_i \quad (35)$$

where, M_i is the molecular weight of species i .

3. Computational Domain and Boundary Conditions

The cases used in the model validation assume the flow to be steady, 2D compressible and reactive flow. The fuel is considered as gaseous hydrocarbon injected from porous wall perpendicular to the main stream. Two gaseous fuels are considered in the present validation and they are propane and methane. For propane combustion, a channel of length, L of 1m and half height, H of 0.05 m is used, as shown in Fig. 1-a. At the lower boundary, a uniform mass flux of 0.21 kg/m²s of premixed propane-air mixture at a temperature of 350K and one atmosphere is injected. While for methane combustion, a channel length of 0.6 m and height of 0.05 m and a uniform mass flux of 0.2 kg/m²s are used. Seven slots are made in the injection surface each of 20mm width for fuel/oxidizer to provide diffusion flame, as shown in Fig. 1-b. The left side of the 2D ducts is closed and no-slip adiabatic wall is considered. The right side is opened to atmosphere at which no gradient in flow parameters exist. While the flow pattern is symmetrical about the axial direction, only half domain is considered as shown in Fig. 1. For turbulence behavior near the wall, details of the used turbulence model are extensively explained in [7].

4. Numerical Treatment

The previously mentioned nonlinear differential equations are solved numerically by using control volume method [13] and the upwind technique as discretization scheme. Demirdzic et al. [14] presented an extended SIMPLE method that implicitly incorporates the influence of pressure on density for simulating compressible flows, and reduces to its standard form in the incompressible flow limit. This extended SIMPLE algorithm will be considered in the present work to ensure pressure-velocity coupling in compressible fluid.

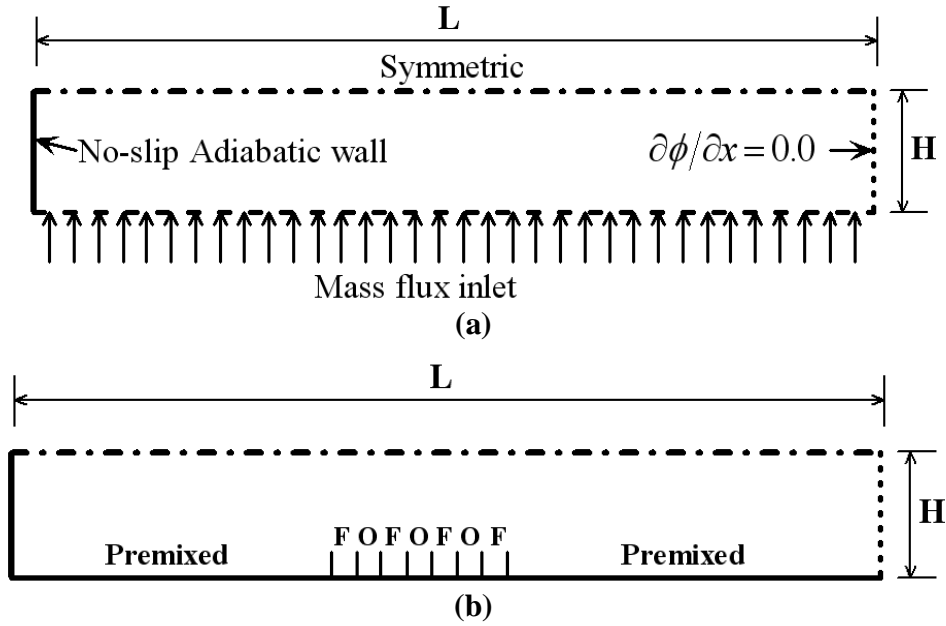


Fig. 1 The boundaries in case of (a) premixed combustion of propane in 2D duct, (b) methane combustion in dual premixed/diffusion configuration

5 Model Validation

In order to validate the model, comparison with other investigators is carried out. Two cases are considered in the present validation. The first case represents the premixed combustion of propane which is injected through porous wall along the entire lower boundary as in [1]. Figure 2 shows the rate of fuel and oxygen consumption inside the reaction zone. Up to 1 mm most of fuel is consumed and the products are fixed at the stoichiometric ratio. This behavior appears clearly in the flame temperature as shown in Fig. 3, where the flame temperature attains its maximum value at the end of the reaction zone. Comparing the result of the present model with that of Tseng et al. [1] and the output of standard FLUENT code V6.3 [9], the figure shows good agreement between the results of the present model with these of FLUENT code as shown in Fig. 3. Both models use the same numerical method (control volume method), while Tseng et al. [1] used the finite different method with pseudo pressure technique to eliminate the probability of singularity. Another comparison with analytical form proposed by [4] shows fair agreement in predicting the maximum temperature as seen in Fig. 4, in spite of the clear slower reaction rate observed in the analytical form output. This behaviour can be attributed to the assumption used in deducing the analytical form which states that the heat release from the exothermic reaction is represented statistically by Gaussian distribution and error function. Moreover, neglecting the axial velocity inside the reaction zone, increases the vertical gas momentum and consequently increases the flame zone as shown in Fig. 4. The analytical form is represented as follows [4]:

$$T(y) = T_w + \frac{2C_1\sqrt{C_3}y + C_2\sqrt{\pi}}{2\sqrt{C_3}\rho v.C_p} \left\{ \text{erf}(C_4\sqrt{C_3}) + \text{erf}\left[\frac{(y - C_4)\sqrt{C_3}}{1}\right] \right\} \quad (36)$$

where, $C_1 = 6.34 \times 10^6$, $C_2 = 1.061 \times 10^9$, $C_3 = 22 \times 10^6$ and $C_4 = 93..251 \times 10^{-5}$

The specific heat for reactant mixture is calculated as follows

$$C_p(T) = \sum Y_i C_{pi} = Y_{C_3H_8} C_{p,C_3H_8} + Y_{O_2} C_{p,O_2} + Y_{N_2} C_{p,N_2} \quad (37)$$

where, Y_i is the mass fraction of species i , and the average specific heat of reactants can be written as follows

$$\bar{C}_p = \frac{1}{T_f - T_w} \int_{T_w}^{T_f} C_p . dt \quad (38)$$

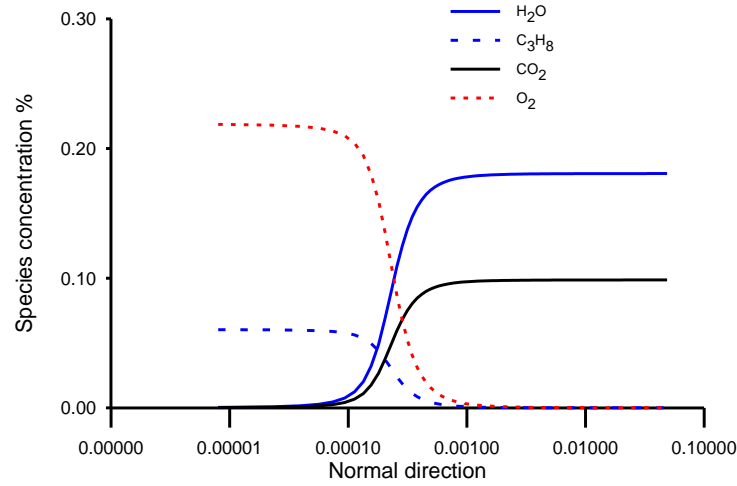


Fig. 2 Species concentration of premixed propane combustion at normal direction.

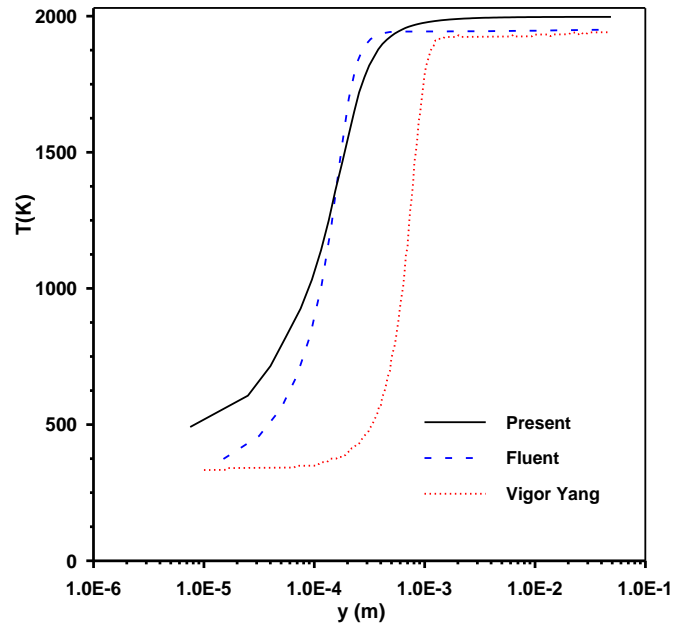


Fig. 3 Temperature distribution in the normal direction inside the reaction zone of propane premixed flame. Comparison between the present model, Vigor Yang model (Tseng et al. [1]) and Fluent code [9]

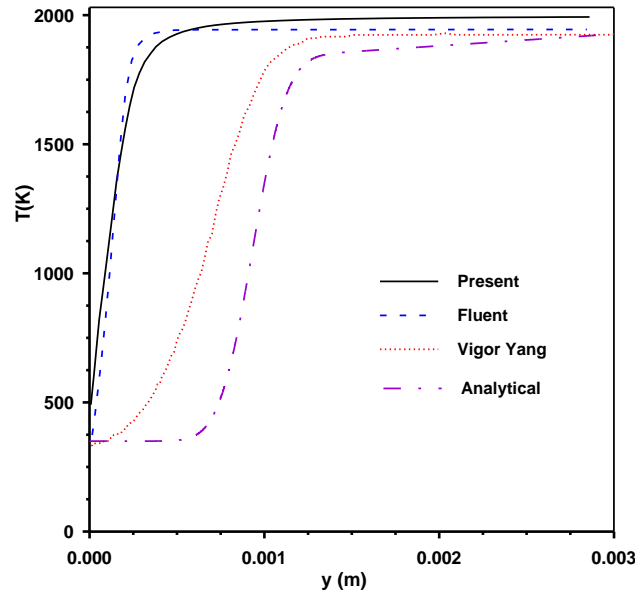


Fig. 4 Temperature distribution in the normal direction inside the reaction zone of propane premixed flame. Comparison between the present model, Vigor Yang model (Tseng et al. [1]) and Fluent code [9] as well as the analytical solution [4]

The second validation test case was established by Chu and Yang [2]. Their computational domain was described previously as shown in Fig. 1.b. It consists of three different gas injection configurations from the porous side walls. The first and the third are premixed combustible mixture. While at the middle is a series of consecutive fuel and oxidizer slots, 20 mm width each and arranged in sandwich type to produce diffusion flame. The premixed combustible mixture is employed to minimize the inconsistency of the temperature field at the interface. The Cartesian grid used in numerical discrimination is 300 (uniformly distributed in axial direction) \times 100 (expanded outward in normal direction). This grid configuration ensures 10 grids to cover each admission slot of fuel or oxidizer gases with spacing equal to 2 mm in the axial direction. The flow of gases inside the chamber is considered as a 2D, compressible, steady and laminar flow. The fuel is methane while the oxidizer is a pure air. Equivalence ratio of the premixed mixture is kept constant and equal to unity. Combustion process is considered as described in equations (20-24) as a single-step kinetic reaction. Comparing the temperature contours inside the computational domain between the present model data and that of Chu and Yang [2], a fair agreement is observed as shown in Fig. 5. Figure 6 represents the temperature gradient along the entire domain. Fig. 6b represents zooming image for the temperature distribution inside the reaction zone around $0.29 <x> 0.33$. Figure 7 illustrates the distribution of fuel concentration inside the entire computational domain. It is shown that, the fuel consumes relatively slower in diffusion combustion compared to the premixed mixture (red zone represents 100 % of fuel while the blue is 0 %).

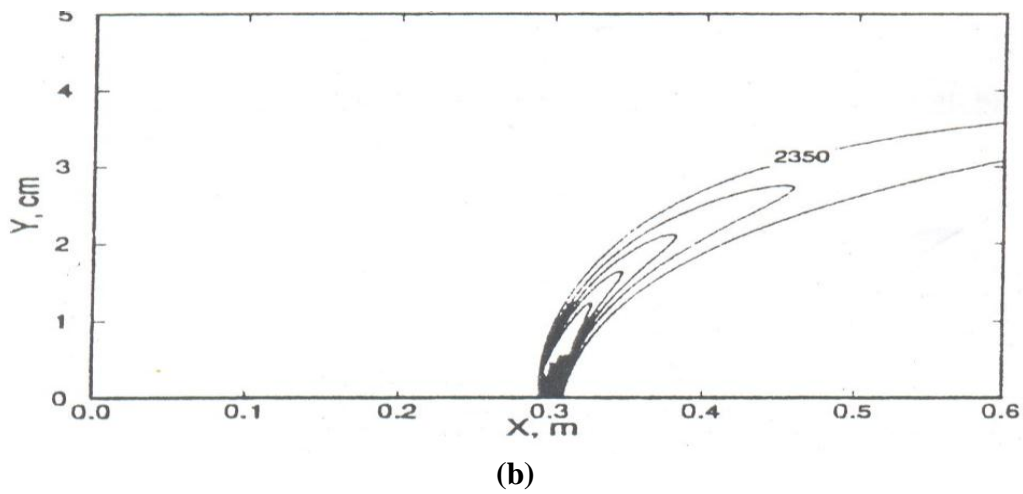
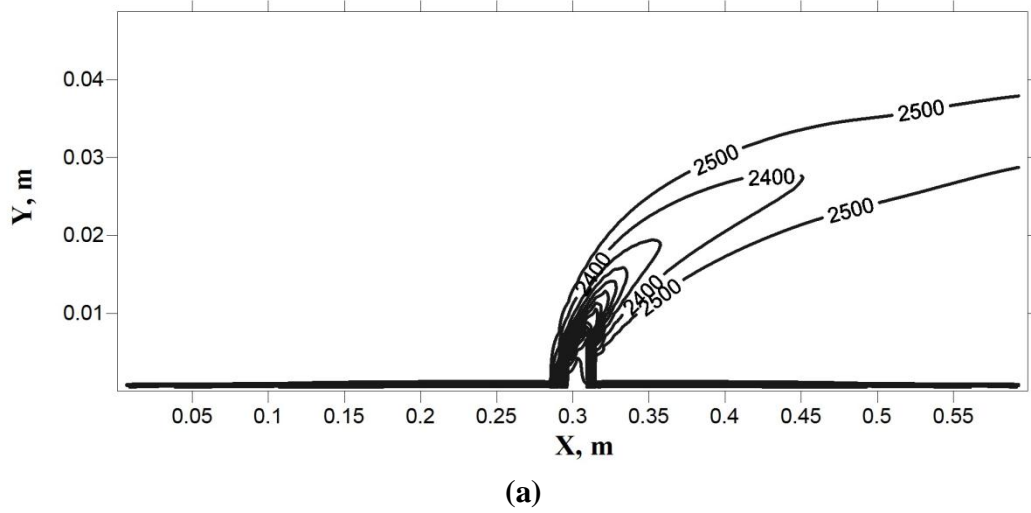


Fig. 5 Temperature distribution in case of diffusion flame using
 (a) the present model (b) the model of Chu and Yang [2]

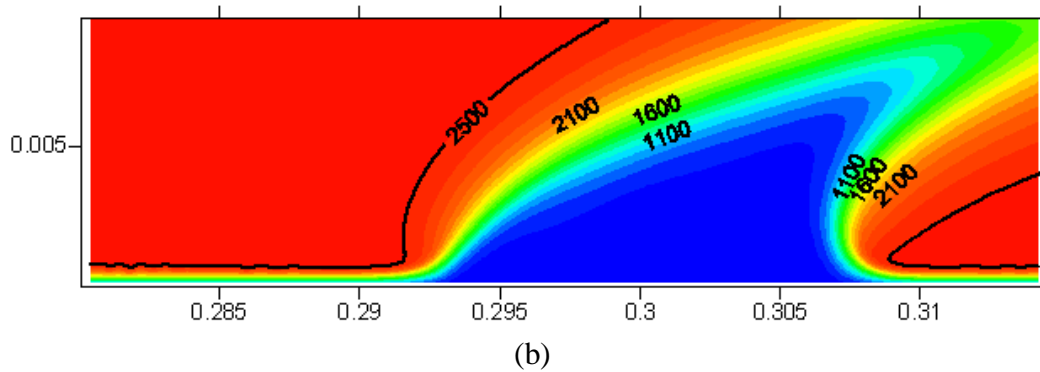
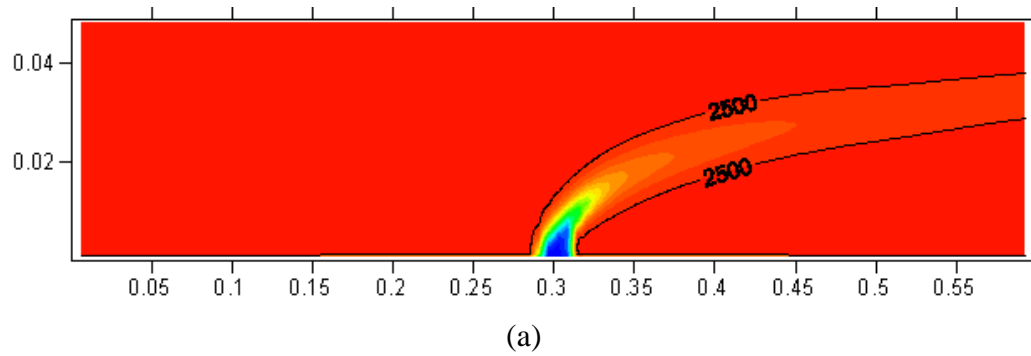


Fig. 6 Temperature distribution along the combustion chamber

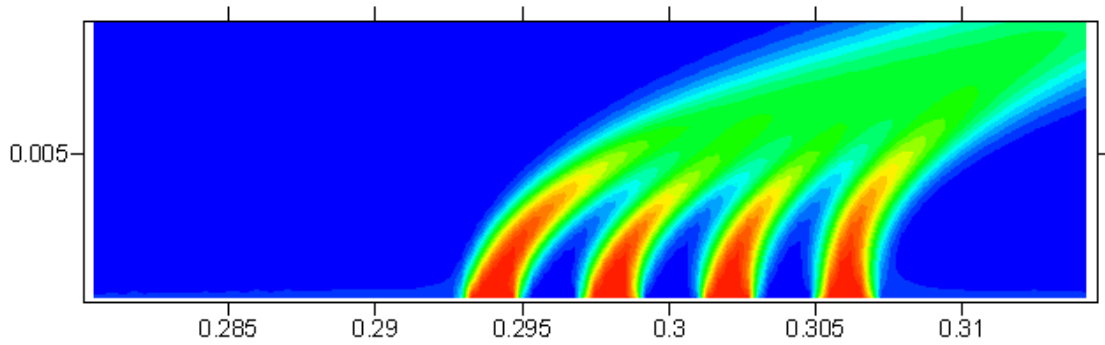


Fig. 7 Fuel concentration distribution along the combustion chamber

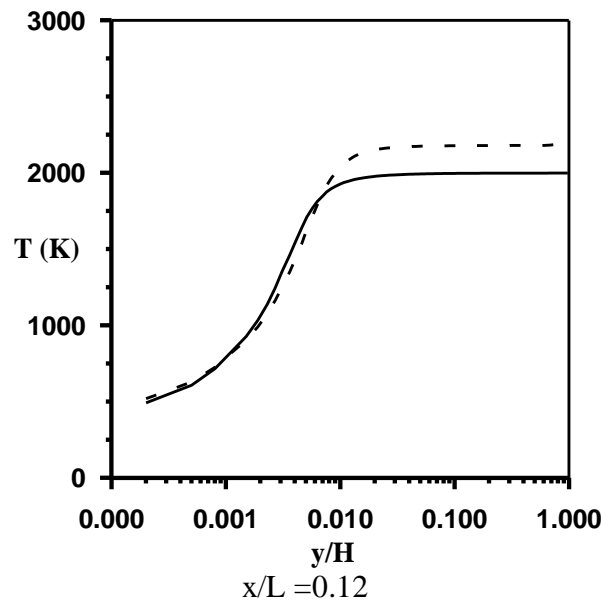


Fig. 8 Comparison between temperature distribution in premixed combustion for laminar and turbulent cases

6. Results and Discussions

In this study different parameters (turbulence intensity, chamber pressure, and the injected mass flux) that may affect the fuel concentration, reaction rate and the temperature inside the combustion chamber are studied. Moreover, the effect of nozzle existence at the end of the chamber on the combustion parameters is introduced.

Figure 8 represents the effect of turbulence on the reaction process. It is found that a slight increase in the flame temperature that accompany with increase in reaction layer thickness as a result of slower reaction rate described in EBU model (equation 34). Data for the proposed test cases are listed in Table (2).

Table (2) Test cases examined in the present study

Mass Flux $\text{kg/m}^2\cdot\text{s}$	Pressure (bar)	Turbulent intensity
0.2*	1*	0.001
0.4	5	0 .01*
1.0	10	0.05

* Base case

The effect of turbulence intensity on the fuel concentration is presented in Fig. 9. Since the great changes occur in the reaction zone above the sandwich model, where the fuel and oxidizer introduced separately, than that above the premixed zone, the results are directed to capture the image above the former one. It is found that, increasing the initial turbulence intensity leads to raise the turbulence kinetic energy inside the flow field which in turn diffuses the reactants over a wide zone above the combustion surface. As a result the life time of fuel inside the reaction zone increases and giving the fuel the opportunity to penetrates deeply inside the combustion chamber. Moreover, this interesting behavior may contribute for another reaction away from the combustion surface if a oxidizer is found there. This trend reflects the behavior of the temperature contours as shown in Fig. 10. Temperature at low turbulence intensity exhibits more uniform distribution compared to the higher turbulence intensity, where the higher turbulence causes a stretching of the flame. As the combustion process is governed mainly by reaction rate, Fig. 11 shows the following: At low turbulence intensity and according to the modified eddy breakup model, Arrhenius law becomes the governing and predominant factor. As a result, the reaction rate in this case becomes nearly temperature dependent. Moreover, it is found that the temperature increases downstream and, in turn, the reaction becomes faster. In case of increasing the turbulence intensity, the rate of fuel dissipation found to be the dominant factor and this behavior is seen clearly on the stretching of the flame downstream as shown in Fig. 11.

The second set of the results represent the effect of injected mass flux and the pressure inside the combustion chamber on the behaviour of combustion process parameters inside the combustion chamber. Figure 12 shows the effect of increasing injected mass flux on the fuel concentration above the combustion surface and how penetrates across the chamber. It is found that, the increase in the injected mass flux from side walls, the vertical velocity component increases accordingly. Therefore, turbulence kinetic energy is increased causing a corresponding intense in turbulent diffusivity. Beside the resultant convective effect when increasing the injected mass flux, the flame lift off and consequently make the reaction zone to be wider than the lower injected mass flux as shown in Fig. 12. The figure shows also slight stretching in flame downstream. This can be attributed to the corresponding increase in vortex stretching downstream. The thicker reaction zone leads to lower fuel concentration gradient as shown in Fig. 13. Therefore, when increasing the mass flux, the heat released from reaction inside diffusion flame zone is distributed along deeper and thinner zone. This appears clearly from temperature contours as shown in Fig 14.

The effect of combustion chamber pressure on the fuel concentration, reaction rate and the temperature is presented in Figs. 15, 16, and 17. Pressure inside the combustion chamber is established as a result of gas production rate from combustion and discharge rate from the nozzle exit. The initial production of combustion gases subsequent to the ignition is greater than the rate of discharge. This contributes to increase the chamber pressure gradually, which defined as the pressure rise period. By the end of this period, balance between the two rates exists and this keeps the pressure at certain level called the operating pressure, until the end of the combustion process. The value of the operating pressure depends mainly on both the fuel factor and geometrical design considerations. When examining the effect of increasing the combustion chamber pressure on the combustion process, it is found that the gas density is increased as a result of increasing the combustion chamber pressure. For constant mass flux injected from the side wall, the relatively heavier gas has lower injection velocity. This in turn leads to reduce the flow field velocity and its turbulent kinetic energy. Finally, the higher chamber pressure will reduce the turbulent diffusivity and leads to squeeze the reaction zone as shown clearly in Fig. 15. Consequently, higher fuel concentration gradient is obtained as shown in Fig. 16. As a result of faster consuming of fuel at higher pressure,

temperature contours exhibits higher gradient in the vertical direction, while the temperature fluctuations at the fuel/oxygen interface is relatively diminished as shown in Fig. 17.

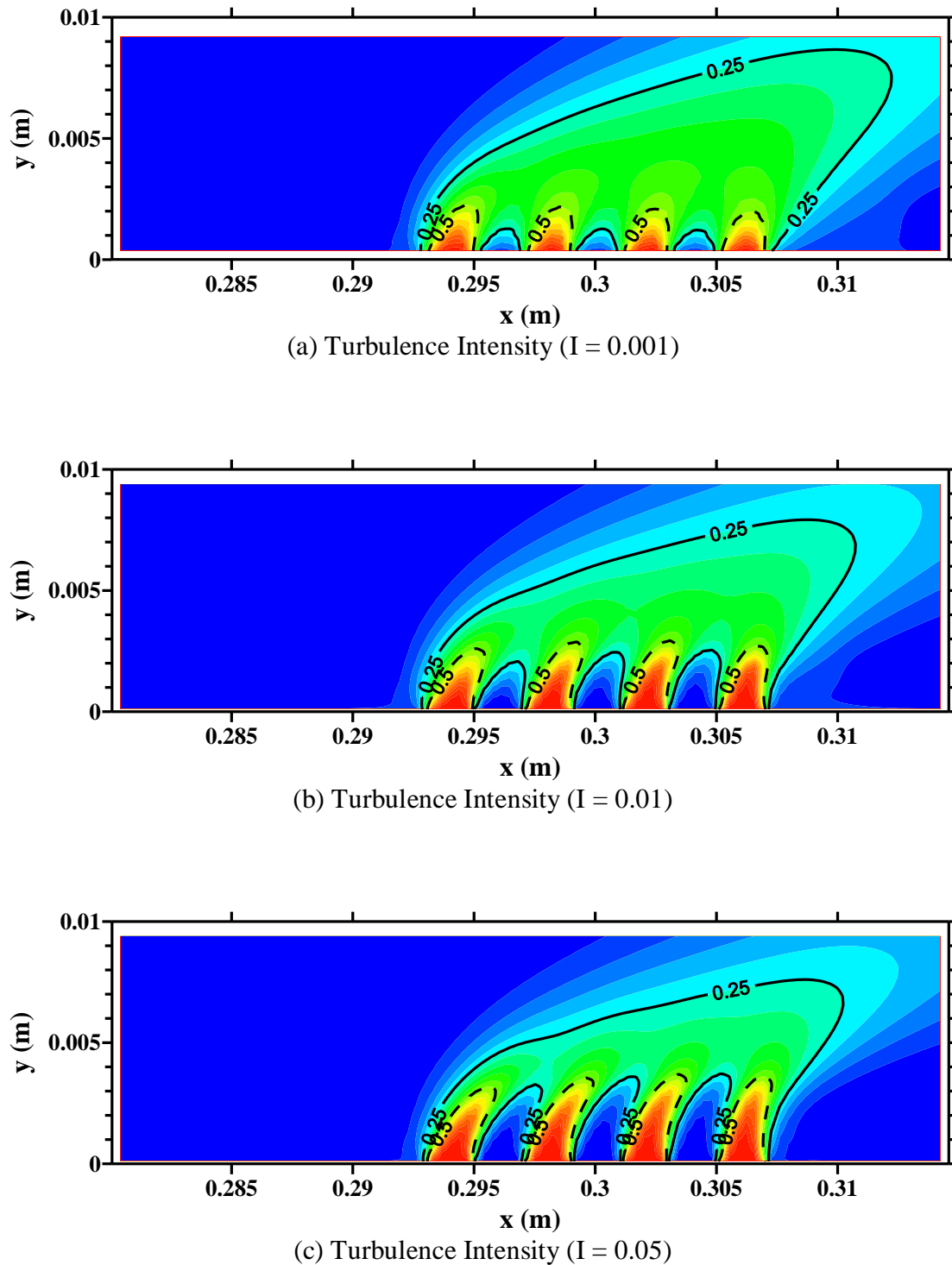
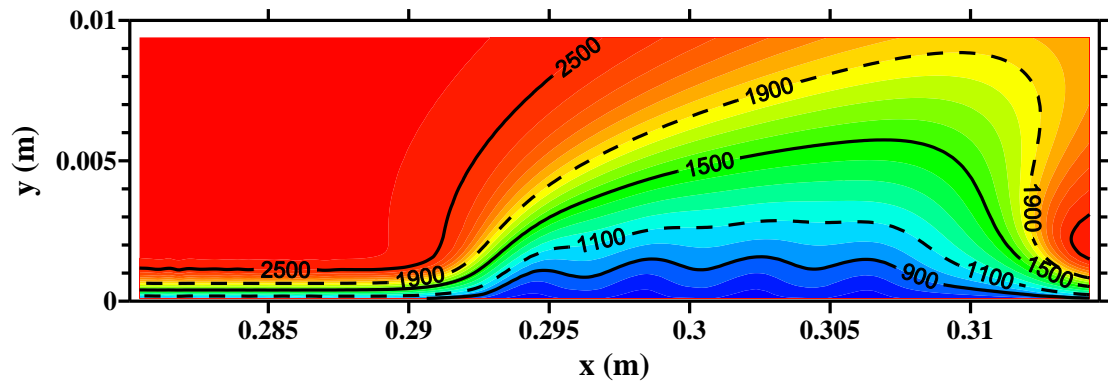
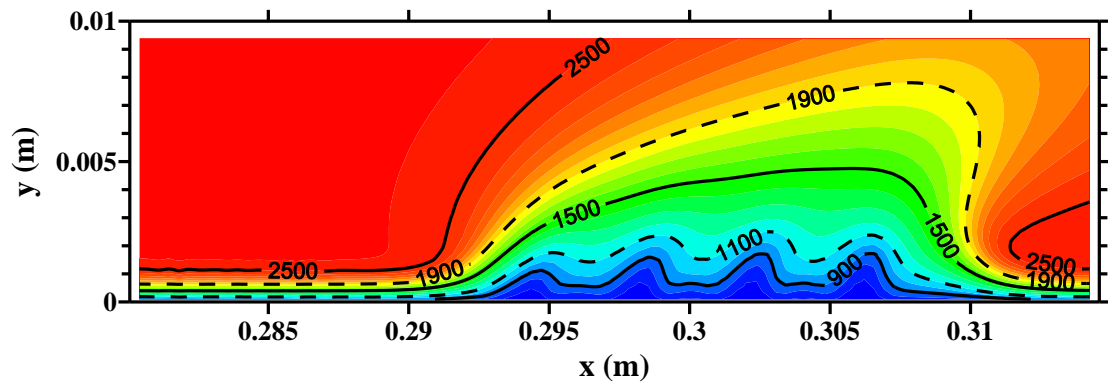
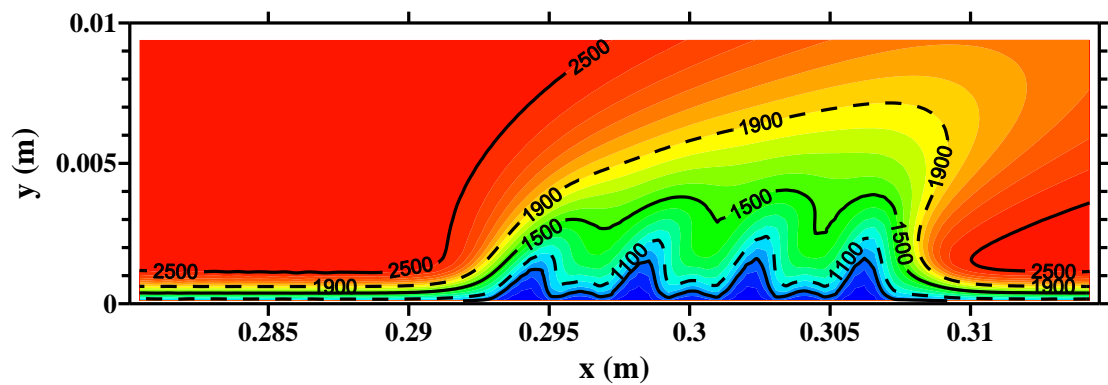
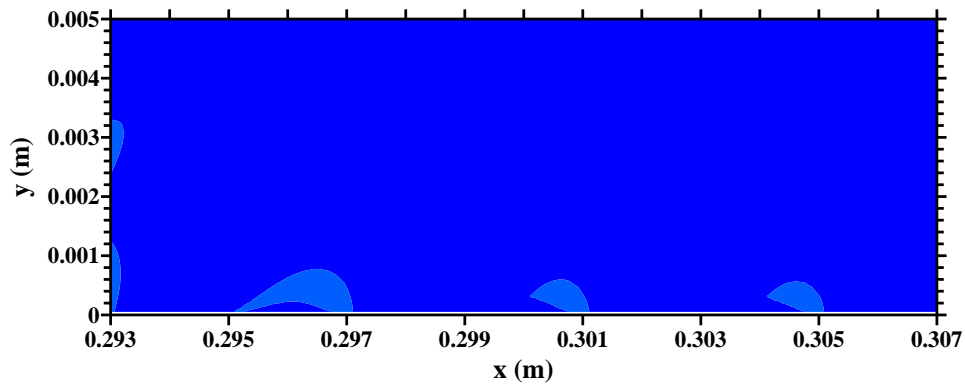
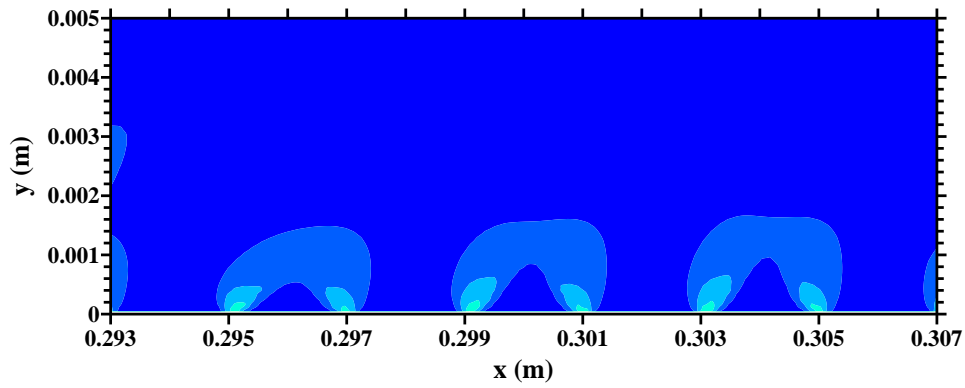
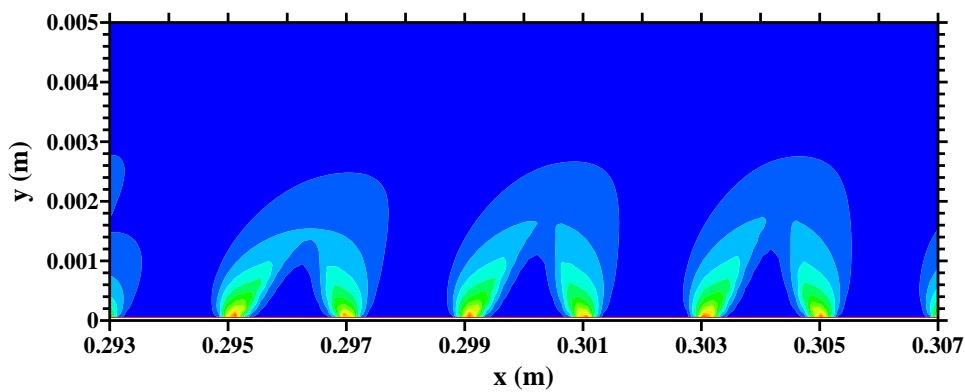


Fig. 9 Fuel concentration contours at different inlet turbulence intensities

(a) Turbulence Intensity ($I = 0.001$)(b) Turbulence Intensity ($I = 0.01$)(c) Turbulence Intensity ($I = 0.05$)**Fig. 10** Temperature contours at different inlet turbulence intensities

Turbulence Intensity ($I = 0.001$)Turbulence Intensity ($I = 0.01$)Turbulence Intensity ($I = 0.05$)**Fig. 11 Fuel reaction rate contours at different inlet turbulence intensities**

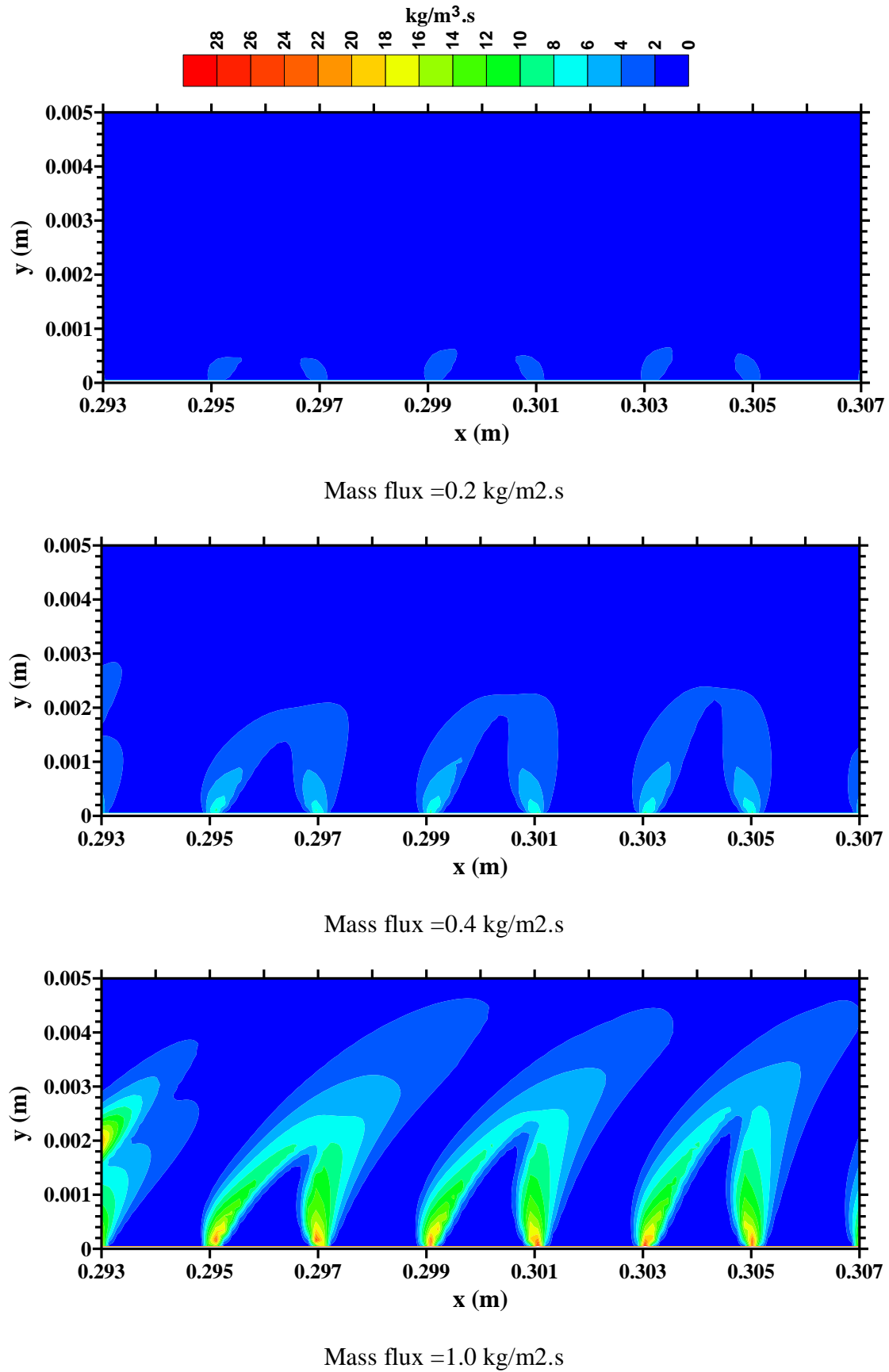
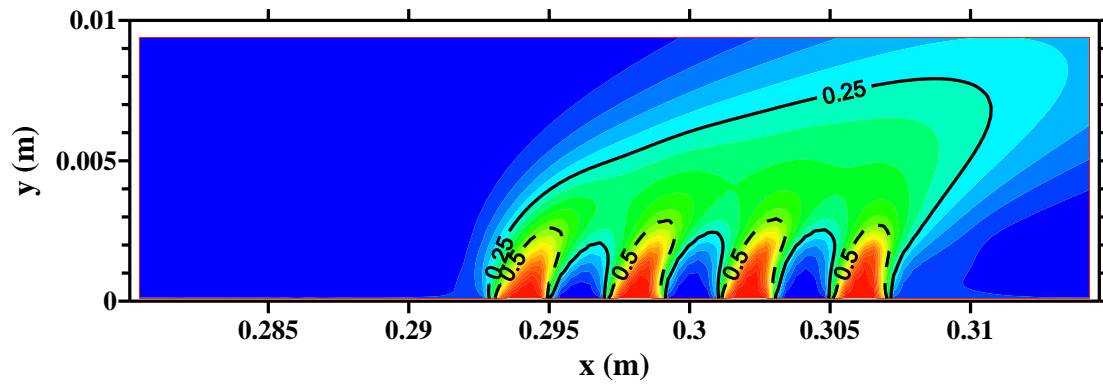
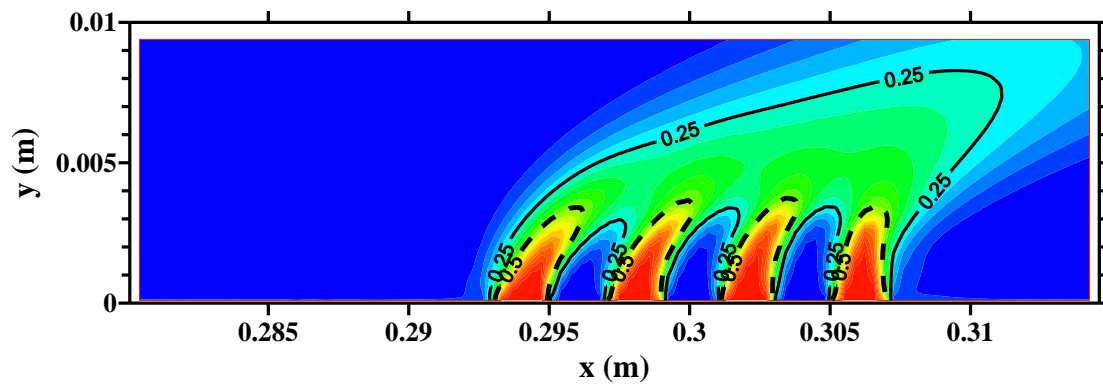


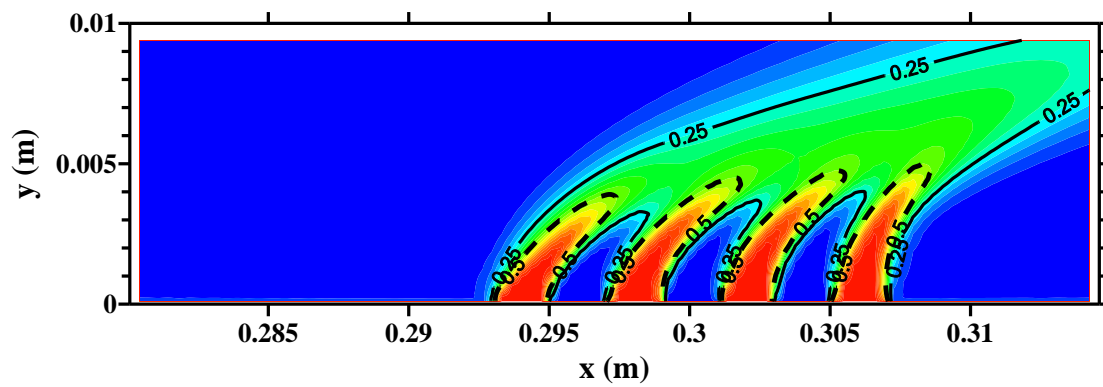
Fig. 12 Fuel reaction rate contours at different mass fluxes



Mass flux = 0.2 kg/m².s

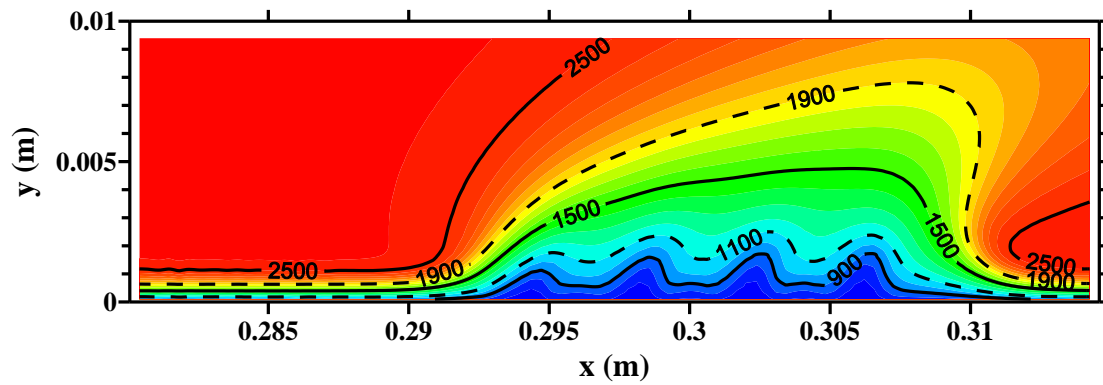


Mass flux = 0.4 kg/m².s

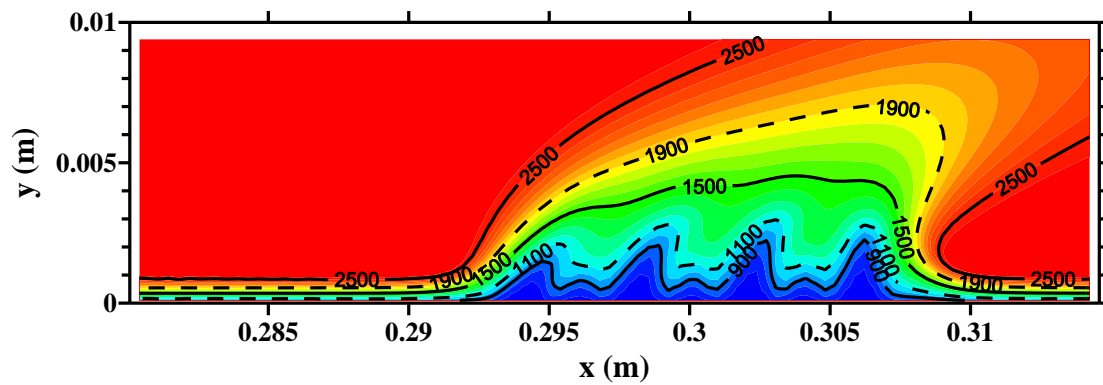


Mass flux = 1.0 kg/m².s

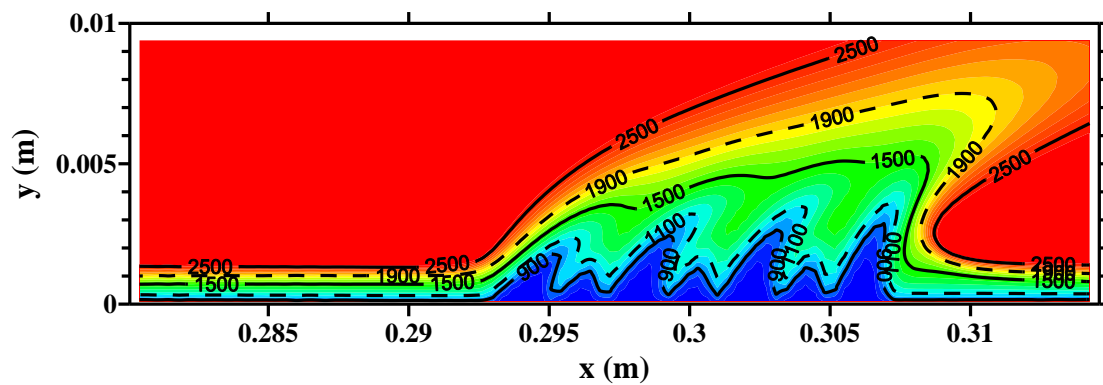
Fig. 13 Fuel concentration contours at different mass fluxes



Mass flux = 0.2 kg/m².s



Mass flux = 0.4 kg/m².s



Mass flux = 1.0 kg/m².s

Fig. 14 Temperature contours at different mass fluxes

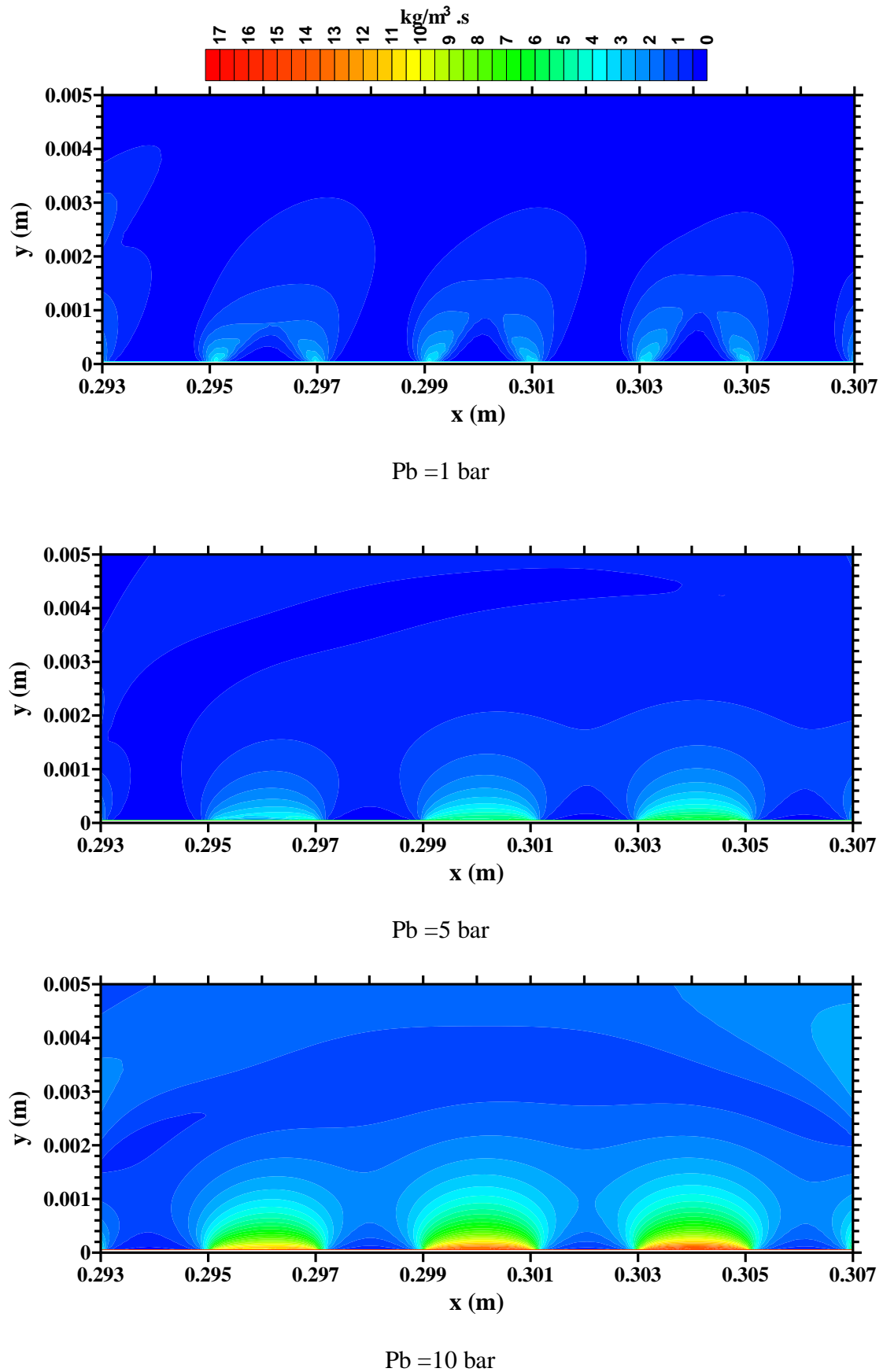
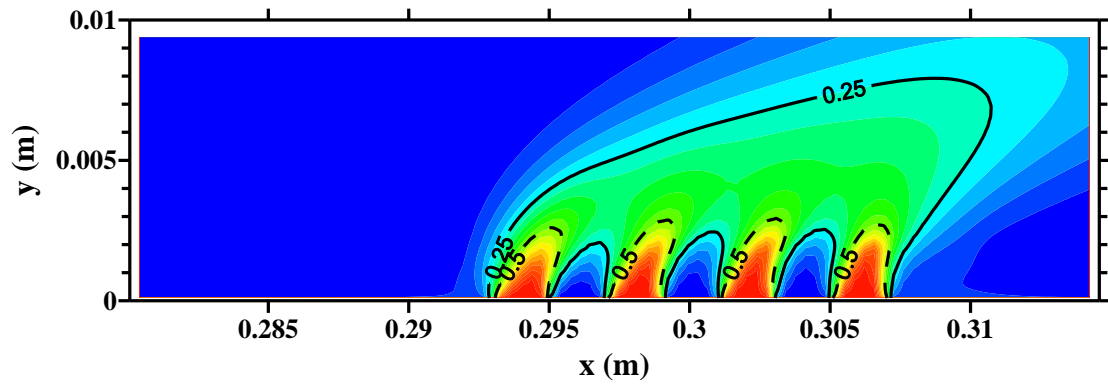
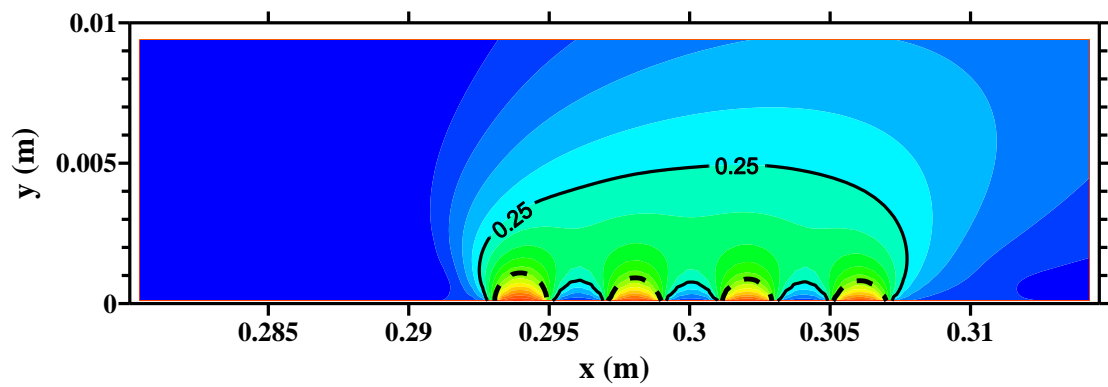


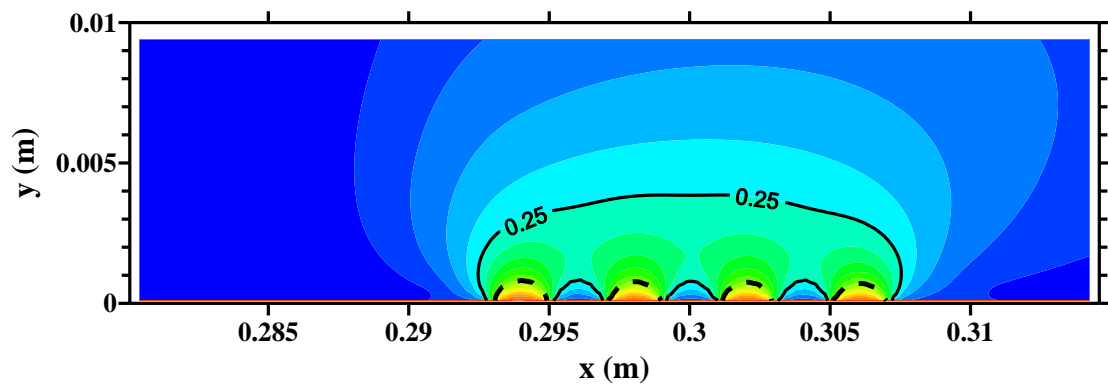
Fig. 15 Fuel reaction rate contours at different back pressures



Pb = 1 bar



Pb = 5 bar



Pb = 10 bar

Fig. 16 Fuel concentration contours at different back pressures

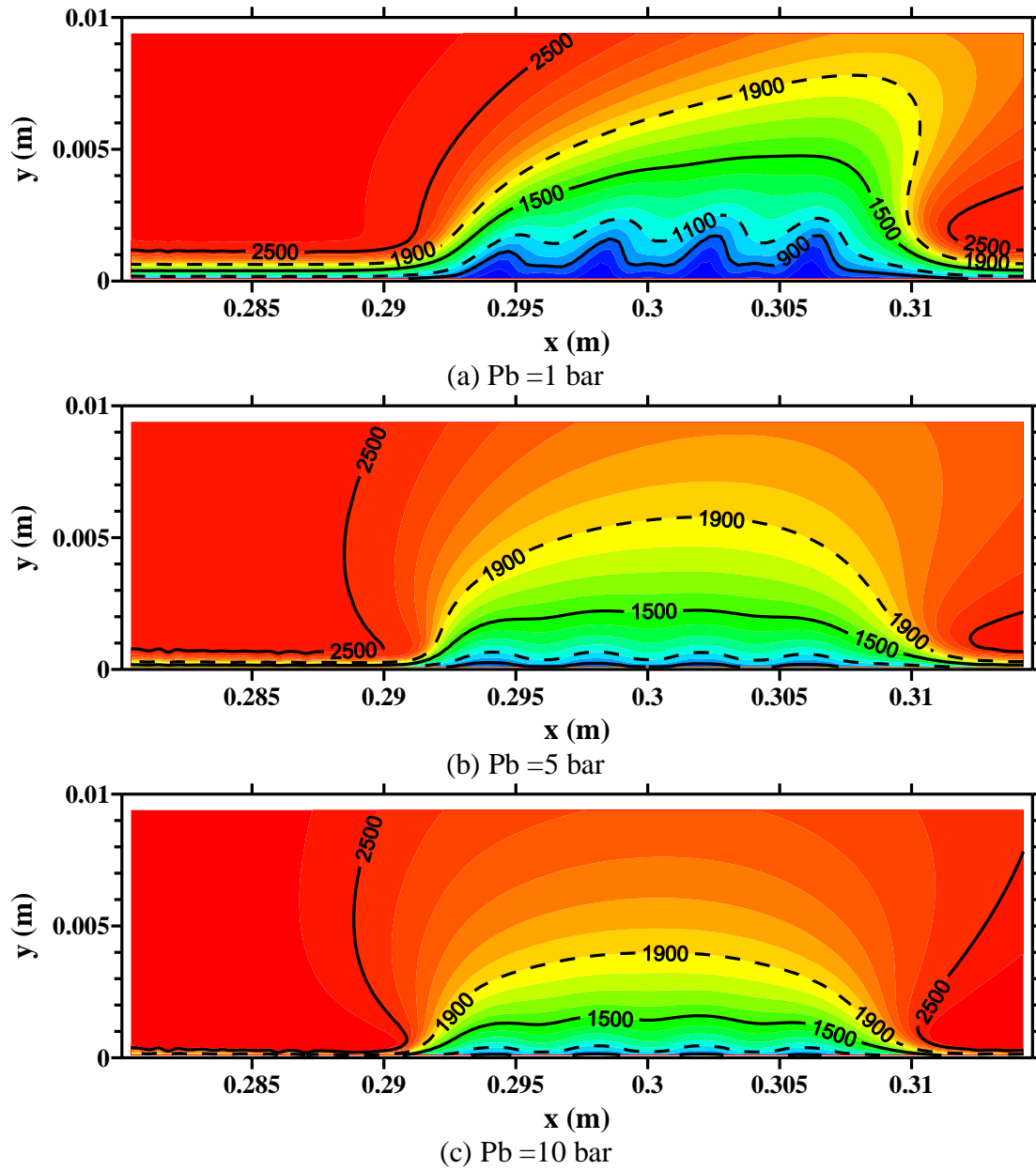


Fig. 17 Temperature contours at different back pressures

The last set of the results is considered in the present work when a nozzle is appended to the combustion chamber. The premixed combustion mode for the mixture injected perpendicularly to the side walls is employed. The base case illustrated in Table (2) is used as input data. The combustion products represented by carbon dioxide concentration along the entire physical domain are illustrated in Fig. 18. The figure shows high gradient inside very thin layer adjacent to the wall at which the combustion takes place. Beyond the flame edge, the products become in equilibrium state and no further change in concentration is obtained. With the progression of the products inside the nozzle and during the expansion process, velocity increases and corresponding stratification of products species takes place. When the mixture leaves the nozzle exit to the rear plenum, the concentration falls rapidly because of the mixing process with the fresh air. Similar gradient for the temperature contours across the combustion chamber and through the nozzle and the rear plenum is represented in Fig.19. It is noted that the temperature attains maximum values in the chamber and gradually decreases as the axial distance increases downstream through the nozzle. In the other side, the fuel

concentration inside the combustion chamber is found to be in a very narrow layer adjacent to the wall at which the fuel consumed rapidly as illustrated in Fig. 20. The results show that the fuel is completely consumed in the combustion chamber and no fuel penetrates through the nozzle.

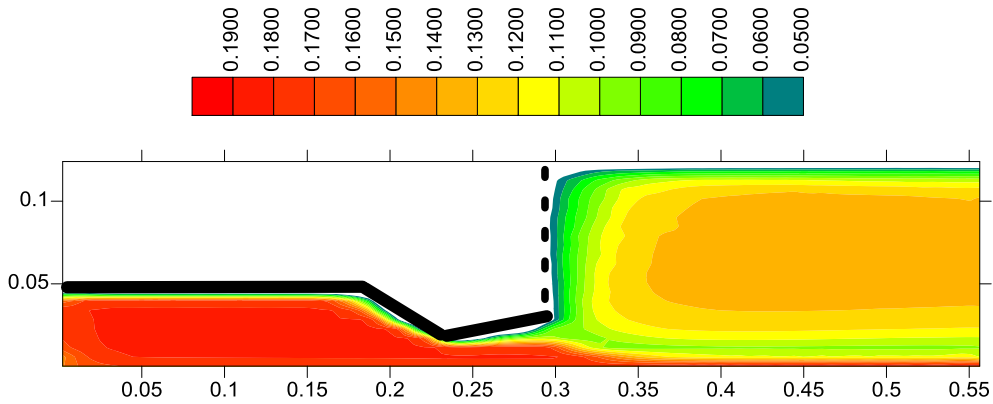


Fig. 18 Variation of CO₂ mass fraction inside a combustion chamber equipped with nozzle.

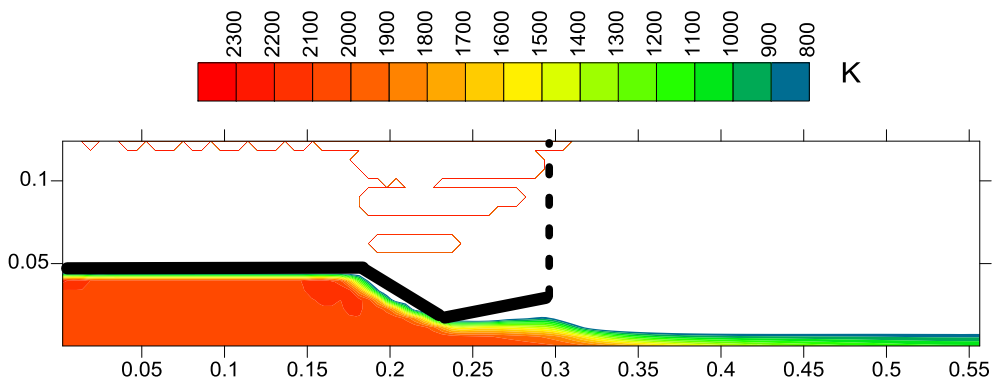


Fig. 19 Temperature distribution inside a combustion chamber equipped with nozzle

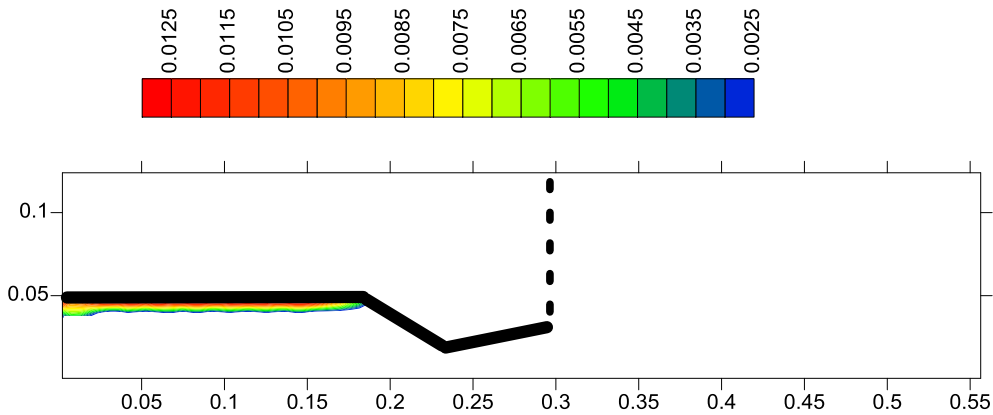


Fig. 20 Variation of fuel mass fraction inside a combustion chamber equipped with nozzle

Finally, the numerical strategy used in this study accounted for the sandwich model for the diffusion flames and the mono-model for the premixed flames. This simulation represents the real life situation of the packed heterogeneous propellant. In spite of this modeling effort for the injected fuel and oxidizer as gases give good insight about the nature of flow fields inside the combustion chamber, but didn't reflect the philosophy of real solid propellant combustion in solid rocket motor. Anyway, the current modeling procedure will pave a road for more intensive computational work to the combustion of heterogeneous solid propellant, accounting for the turbulent, multi-dimensional gas phase physics, the solid phase physics and an unsteady non-planar description of the regressing propellant surface as extension to the laminar consideration by Hegab et.al. [15,16] and Hegab and Balabel [17] for the long scale instead of the microscale modeling. Moreover, more intensive computational work is needed to study the effects of turbulent cross-flow in solid rocket motor chamber on the burning rate of a real long scale multimodal composite propellant instead of the cold one as Hegab and Kassoy, [18].

7. Conclusion

In the current study, a comprehensive mathematical model is developed to simulate the turbulent combustion inside SRM combustion chamber. This model is based on solving strongly coupled set of partial differential equations representing the conservation of mass, momentum, species transport and energy as well as the two equations for turbulence. Eddy breakup model is used to account the effect of turbulence on the finite rate of reaction. The output results of the model are compared with another data for different combustion modes with no nozzle. The comparison shows fair agreements. The model is then used and extended to study different cases to draw the following conclusion points. At low turbulence intensity, combustion is governed by Arrhenius law, while at high turbulence intensity; the rate of fuel dissipation becomes the dominant factor. Increasing the injected mass flux through side wall injection leads to the same combustion behavior at high turbulence intensity. When combustion occurs at high pressure, density will increase and this contributes for inhibiting the effect of turbulent diffusivity and squeezes the reaction zone. Moreover, the combustion parameters in case of nozzle existence are illustrated to capture full image about the reactive fluid dynamics behavior through the chamber, nozzle, and the rear plenum. In general, the steady state combustion turbulent modeling gave a good insight about the nature of the complex fluid flow in simulated solid rocket motor chamber, but didn't reflect the perturbed generated combustion products of real composite propellant. As a result, more intensive computational work is needed to study the effects of turbulent oscillated cross-flow in solid rocket motor chamber on the burning rate of a real long scale multimodal composite propellant.

Acknowledgment

This work is supported by the Science and Technology Development Fund (STDF) through the project STDF-ID-108.

References

- [1] Tseng, C-F, Tseng, I. S., Chu, W. W. and Yang V. "Interactions between Acoustic Waves and Premixed Flamed in Porous Chambers" AIAA paper No. 94-3328, 1994.
- [2] Chu, W. W. and Yang V. "Dynamic Responses of Diffusion Flames to Acoustic Oscillations in a Simulated Solid Rocket Motor" AIAA paper No. 96-0883, 1996.
- [3] Westbrook, C. K. and Dryer F. L. "Simplified Reaction Mechanisms for Oxidation of Hydrocarbon Fuels in Flames" Combustion Science & Tech., Vol. 27, pp. 31-43, 1981.

- [4] Vyas, A.B, Majdalani, J and Yang V. "Estimation of Laminar Premixed Flame Temperature and Velocity in Injection Driven Combustion Chambers" *Combustion and Flame*, Vol. 133, pp. 371-374, 2003.
- [5] Cherng D. L., Yang V. and Kuo K. K. "Numerical Study Of Turbulent Reacting Flows in Solid Propellant Duct Rocket Combustors" *AIAA J. of Propulsion*, Vol. 5, No. 6, pp. 678-685, 1989.
- [6] Lien F.S. and Kalitzen G. "Computation of Transonic Flow with the $v^2 - f$ Turbulence Model", *International Journal of Heat and Fluid Flow*, Vol. 22, pp. 53-61, 2001.
- [7] El-Askary W.A., Balabel A., El-Behery S.M. and Hegab A. "Prediction of Turbulence Transpiration Resulting from Asymmetric and Symmetric Mass Injection in a Porous Channel" ICFD10-EG-3070, Tenth International Congress of Fluid Dynamics, December 16-19, 2010, Stella Di Mare Sea Club Hotel, Ain Soukhna, Red Sea, Egypt.
- [8] Heywood, J. P. "Internal Combustion Engines Fundamentals" Mc.Graw Hill, 1986.
- [9] Fluent 6.3 manual, Fluent Inc., Lebanon, USA, 2006.
- [10] Srinivasan R., Reynolds R., Ball I., Berry R., Johnson K. and Mongia H. "Aerothermal Modeling Program" NASA-N84-12265, Aug. 1983.
- [11] Spalding D. B. "Mixing and Chemical Reaction in Steady, Confined Turbulent Flames" 13th Symposium on Combustion, pp. 649-657, 1971.
- [12] Spalding D. B. "Development of Eddy-Breakup Model of Turbulent Combustion" 16th Symposium on Combustion, p. 1657-1663, 1976.
- [13] Patanker S. V. "Numerical Heat Transfer and Fluid Flows" Hemisphere, New York, 1980.
- [14] Demirdzic, I., Lilek, Z. and Peric, M. "A Collocated Finite Volume Method for Predicting Flows at all Speeds" *Int. J. Num. Met. Fluids*, Vol. 17, pp. 1029-1050, 1993.
- [15] Hegab A., Jackson T., Buckmaster J., Stewart D., (2001) "Nonsteady Burning of Periodic Sandwich Propellants with Complete Coupling between the Solid and Gas Phases", *Journal of Combustion and Flame*, 125, 1055-1070, 2001.
- [16] Hegab A., Buckmaster J., Jackson T., and Stewart, S. "The Burning of Periodic Sandwich Propellants" AIAA Paper 2000-3459, 36th. AIAA/ASME/SAE/ASEE Joint Propulsion, July 17-19, 2000, Huntsville, AL, USA.
- [17] Hegab, A.M. and Balabel, A. . " Effect of Ammonium Perchlorate Grain Sizes on the Combustion of Solid Rocket Propellant" *Proceeding of the 12-th Aerospace Science & Aviation Technology Conference, (ASAT-12), 29-31 may 2007, CHA-1, pp 1-20, Military Technical College, Cairo, Egypt.*
- [18] Hegab, A.M., and Kassoy, D.R., (2006) "Internal Flow Temperature and Vorticity Dynamics Due to Transient Mass Addition", *AIAA Journal*, Vol.44, No.4, April 2006.